Popular Integration Grids Can Result in Large Errors in DFT-Computed Free Energies

Andrea N. Bootsma and Steven E. Wheeler*

Center for Computational Quantum Chemistry, Department of Chemistry, University of Georgia, Athens, GA 30602
E-mail: swheele2@uga.edu

Abstract

Density functional theory (DFT) has emerged as a powerful tool for analyzing (bio-)organic and organometallic systems and proved remarkably accurate in computing the small free energy differences that underpin many chemical phenomena (*e.g.* regio- and stereoselective reactions). We show that the lack of rotational invariance of popular DFT integration grids reveals large uncertainties in computed free energies for some isomerizations, torsional barriers, and regio- and stereoselective reactions. The result is that predictions based on DFT-computed free energies for systems with very low-frequency vibrational modes can change qualitatively depending on molecular orientation. For example, for a metal-free propargylation of benzaldehyde, predicted enantioselectivities based on B97-D/def2-TZVP free energies using a popular pruned (75,302) integration grid can vary from 62:38 to 99:1 by simply rotating the transition state structures. Relative free energies for the regiocontrolling transition state structures for an Ir-catalyzed C–H functionalization reaction computed using M06/6-31G(*d*,*p*)/LANL2DZ and the same grid can vary by more than 5 kcal mol^{-1}, resulting in predicted regioselectivities that range anywhere from 14:86 to >99:1. Errors of these magnitudes occur for different functionals and basis sets, are potentially widespread among modern applications of DFT, and can be reduced by using much denser integration grids than commonly employed.

Introduction

Density functional theory (DFT) is widely used to understand and predict the properties and reactivity of complex (bio-)organic and organometallic systems,[1-9] particularly among non-experts. Many of these applications require accuracies in relative free energies (ΔG or ΔΔG) that are smaller than the quantities of interest, which are often only a few kcal mol^{-1}. For instance, in the context of regio- and stereoselective reactions, a 1 kcal mol^{-1} change in relative free energy barriers can be the difference between modest and high selectivity.[3] . Several recent reviews have highlighted the many challenges faced in achieving such accuracy,[2,10-12] and errors arising from the choice of DFT functional and basis set are widely appreciated among users. However, there is an additional source of potentially significant errors in DFT free energies that goes largely unnoticed—the integration grid.

The evaluation of integrals over the exchange-correlation potential in DFT requires a numerical integration scheme, which is accomplished in most quantum chemistry programs using atom-centered grids comprising N^r shells of N^Ω points denoted as (N^r,N^Ω). Integration grid errors can significantly impact energies and other molecular properties, particularly for newer functionals.[10,13-28] For example, in 2010, Wheeler and Houk[24] reported large grid errors in isomerization energies of small organic molecules when members of the M06 suite of functionals[29] were paired with the SG-1 grid [a pruned (50,194) grid].[30] In 2016, Head-Gordon and co-workers[26] assessed grid errors across a wider array of Minnesota functionals, finding that atomization energies are often converged with a (75,302) grid (similar to the 'fine' grid in Gaussian) for all but two of these functionals and fully converged for all of them with a (99,590) grid (*i.e*. an 'ultrafine' grid). In light of the grid sensitivity of electronic energies from some DFT functionals, there have been recent efforts to account for this in the development and (re)parameterization of DFT functionals[25,27-28,31] and Herbert *et al*.[32] have developed standardized grids designed to provide accurate energies for modern DFT functionals.

These previous discussions of grid errors primarily concerned electronic energies. Here, we show that popular grids can lead to even larger errors in *free energies*, with harrowing implications for DFT studies of organic and organometallic systems. These errors arise from the sensitivity of the entropic component of the free energy to small variations in the values of low-frequency vibrational modes but are distinct from errors due to the treatment of these modes as harmonic oscillators. Moreover, they occur using different DFT functionals and basis sets and require at least a (99,590) grid to be resolved in many cases.

Results and Discussion

In the absence of an external field, the energy of a molecule should be independent of its orientation relative to the lab-fixed Cartesian coordinate system. However, because the atom-centered integration grids used in most quantum chemistry packages are anchored to the Cartesian axes, DFT energies typically lack invariance with respect to rigid-body rotations. While this has been known for decades,[30,33-35] some users are not aware of this shortcoming because many quantum chemistry codes automatically reorient molecules such that the principle axes are aligned with the Cartesian axes (the so-called 'standard orientation'). Luckily, this lack of rotational invariance has negligible impact on relative electronic energies, at least for small systems and some DFT functionals (*vide infra*). For instance, the B97-D/def2-TZVP electronic energy (E) of 2-butyne relative to 1,3-butadiene (reaction 1) is plotted in Figure 1A as a function of the rotation of 2-butyne around an axis perpendicular to the molecule using a pruned (75,302) grid. The variation in this relative energy is 0.01 kcal mol^{-1}.

However, first and second derivatives of the DFT energy with respect to nuclear displacements also lack rotational invariance. The result is that both the geometries of stationary points and the values of harmonic vibrational frequencies depend on the molecular orientation. For example, in the case of 2-butyne, the B97-D/def2-TZVP value for the methyl rocking mode using a pruned (75,302) grid, which is the default in Gaussian09[36] and has been recommended by Herbert *et al*.[32] for B97-derived functionals, varies from 31*i* to 29 cm^{-1} upon rotation (see Figure 1B). In other words, the very nature of this stationary point on this DFT potential energy surface depends on the molecular orientation, even if the geometry is tightly optimized at each orientation. In terms of zero-point vibrational corrected energies and thermal enthalpies, such fluctuations in low-frequency vibrational modes are typically inconsequential (if one excludes orientations for which there is an anomalous imaginary mode). On the other hand, the impact on free energies is substantial due to the sensitivity of the entropic component to small vibrational frequencies within the standard rigid-rotor/harmonic-oscillator (RRHO) approximation. For example, using this (75,302) grid and excluding the orientations for which the low-frequency mode is imaginary, there is ~1 kcal mol^{-1} variation in ΔG for reaction 1 (see Figure 1A).

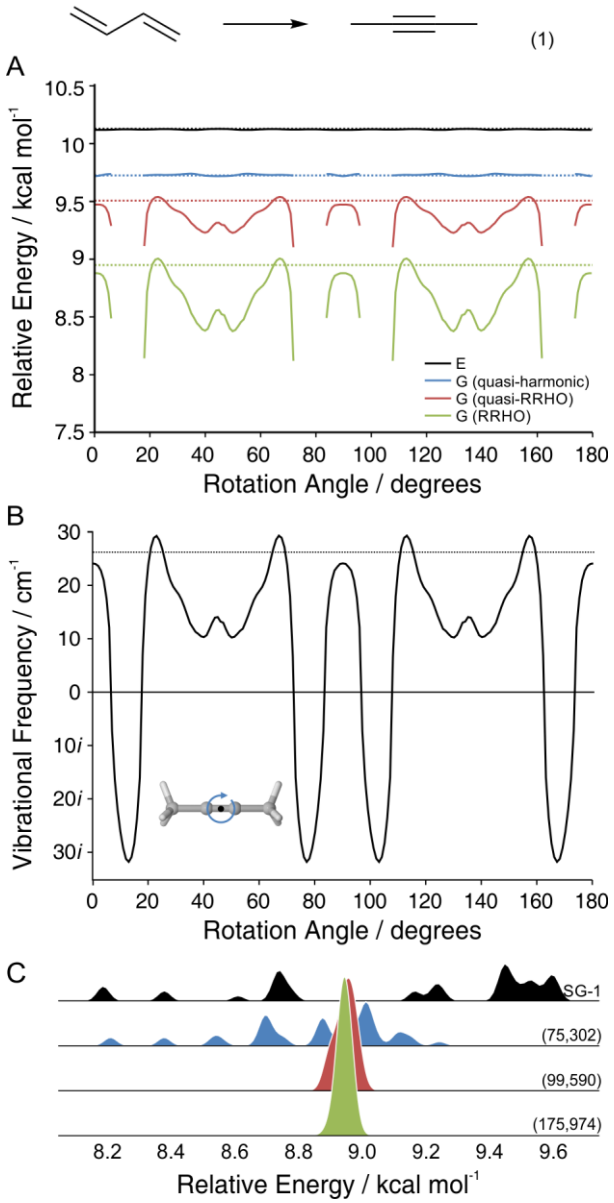

Figure 1. A) B97-D/def2-TZVP energy (E) and free energy (G) of reaction 1 as a function of rotation of D_{3h}-symmetric 2-butyne around the indicated axis using a (75,302) grid. Free energies for orientations at which the low-lying frequency is imaginary are omitted. The grid-converged values are indicated with dotted lines. B) Low-frequency vibration for 2-butyne as a function of the indicated rotation using a (75,302) grid. The grid-converged value is indicated with a dotted line. C) Distribution of RRHO free energies for reaction 1 across 50 representative orientations using four popular integration grids.

Variations in both vibrational frequencies and free energies exhibit a 90° periodicity (see Figures 1A and B), mirroring the octahedral symmetry of the atom-centered grids.[37] To assess how these errors behave for different grids, the distribution of free energies for reaction 1 across 50 representative orientations of 2-butyne are plotted for four popular integration grids in Figure

1C. The extent of variations in ΔG contracts with increasing grid size, and by the (99,590) grid becomes negligible. In other words, the lack of rotational invariance can be used as a gauge of the grid errors for a given free energy difference. Similar variations occur using other functionals and basis sets [see SI Figure S1 for data using B97-D,[38-39] B3LYP,[40] PBE,[41] ωB97X-D,[42] and M06-2X[43] paired with 6-31G(d), cc-pVTZ, and def2-TZVP][44-45] and different electronic structure packages.[46]

Of course, the real culprit is the RRHO approximation, which should not be used for low-frequency vibrational modes. Instead, these modes should be projected out of the hessian and treated separately as, for example, hindered rotors.[47-50] While such treatments are feasible for simple molecules such as 2-butyne, they are impractical for the large systems on which DFT methods are most often applied because the problematic modes rarely involve simple combinations of internal coordinates. Instead, users tend to employ more approximate treatments of the entropic contribution of low-frequency vibrations. Chief among these are the quasi-harmonic approximation of Cramer and Truhlar[51] and the quasi-RRHO approximation of Grimme.[52] In the former, vibrational frequencies below some cutoff value (typically 100 cm^{-1}) are changed to that cutoff value and the RRHO formulae applied. In the latter, the entropic contributions of vibrational frequencies below some cutoff (again, typically 100 cm^{-1}) are interpolated between those from an effective free-rotor and the RRHO limit. Figure 1A shows that the use of the quasi-RRHO approach reduces variations in ΔG for reaction 1 by limiting the impact of low-frequency vibrations. The quasi-harmonic approximation all but eliminates these variations because the most problematic mode is consistently below the cutoff value, so is shifted to a constant value of 100 cm^{-1}. However, grid errors in quasi-harmonic free energies will remain in cases in which one or more vibrational frequencies exhibit variability around the cutoff value (*vide infra*).

Such grid errors are not isolated to reaction 1 but will occur for any transformation in which one or more molecules exhibit low frequency vibrational modes.[53] This includes many of the organic and organometallic molecules studied using DFT,[1-9] which tend to exhibit large-amplitude rocking motions with very low frequencies (<50 cm^{-1}). Moreover, variations in DFT-computed free energies upon rotations can be substantial, resulting in uncertainties in free energies that can overshadow quantities of interest. Scheme 1 shows four systems that highlight the potential impacts of these grid errors, spanning a range of molecular sizes and complexities. Reaction 2 concerns the relative free energy (ΔG) of the atropisomeric HIV integrase inhibitor **1**

and its diastereomer (**1′**),[54] while quantifying the rate of reaction 3 requires the torsional free energy barrier ($\Delta G^{\ddagger}$) of 4,4′-dimethyl-1,1′-biphenyl. Predicting the selectivity of reactions 4 and 5 requires relative free energies ($\Delta\Delta G^{\ddagger}$) for competing transition state (TS) structures leading to alternative products. In particular, the stereoselective addition of allenyltrichlorosilane to benzaldehyde catalyzed by a 2,2′-biquinoline-*N*,*N*′-dioxide[55-58] (reaction 4) depends on the relative free energy of TS structures leading to enantiomeric products. In reaction 5, Ir can catalyze the C–H functionalization of indole at either C_2 or C_7 depending on the relative free energy of the corresponding TS structures.[59] Free energy swings of ±2 kcal mol^{-1} can be catastrophic for predicting the outcome of reactions such as 4 and 5 because of the exponential dependence of selectivities on $\Delta\Delta G^{\ddagger}$.[3] For each of these transformations, we quantified uncertainties in the energy, enthalpy, and free energy due to integration grid errors by sampling representative orientations, fully optimizing the geometry for each orientation (see Computational Methods for details).

Scheme 1. Representative transformations for which accurate relative free energies are required.

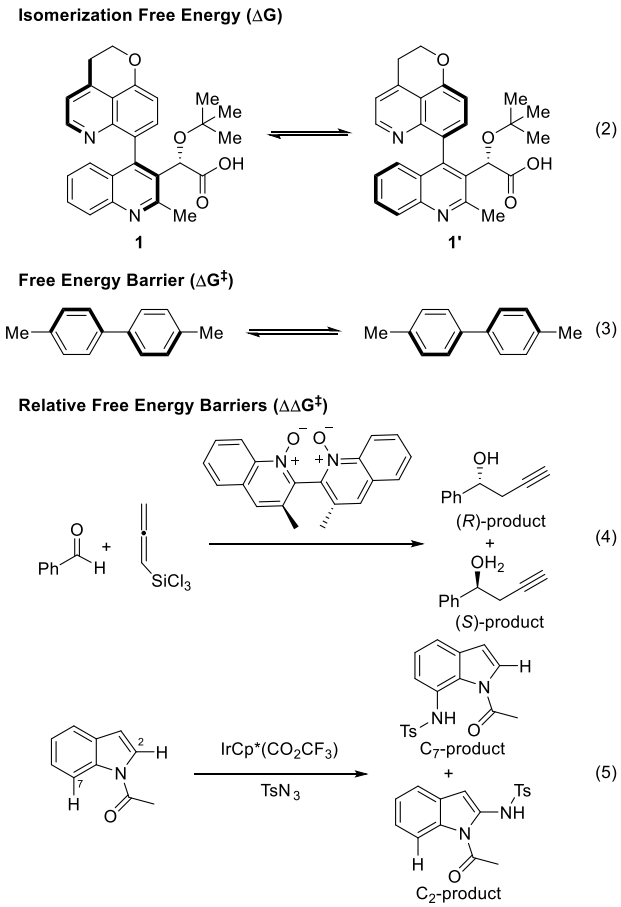

Table 1. Grid converged energy, enthalpy, and free energy differences and minimum and maximum values across representative orientations for four pruned integration grids for reactions 1-5, in kcal mol^{-1}.

Reaction	Grid Converged Value[a]	SG-1		(75,302)		(99,590)		(175,974)	
		Min	Max	Min	Max	Min	Max	Min	Max
Electronic Energy									
(1)	10.1	10.1	10.2	10.1	10.1	10.1	10.1	10.1	10.1
(2)	1.1	0.7	1.5	0.9	1.2	1.1	1.1	1.1	1.1
(3)	2.0	1.6	2.2	1.9	2.0	2.0	2.0	2.0	2.0
(4)	0.5	-0.2	1.2	0.3	0.8	0.5	0.6	0.5	0.5
(5)	1.3	0.1	2.0	0.9	1.6	1.2	1.4	1.3	1.3
Enthalpy (298K)									
(1)	10.0	10.0	10.0	10.0	10.0	10.0	10.0	10.0	10.0
(2)	1.1	0.6	1.5	0.9	1.4	1.0	1.2	1.0	1.1
(3)	1.4	1.2	2.8	1.3	1.5	1.3	1.4	1.4	1.4
(4)	0.7	0.1	1.2	0.6	0.9	0.6	0.7	0.6	0.7
(5)	1.2	0.1	3.0	0.8	2.1	1.1	1.5	1.2	1.3
Free Energy (RRHO Approximation)									
(1)	8.9	8.2	9.6	8.4	9.2	8.9	9.0	8.9	9.0
(2)	0.7	-0.6	2.8	0.0	2.4	0.5	1.5	0.4	1.1
(3)	2.6	1.0	3.3	0.8	3.5	2.4	3.1	2.5	2.8
(4)	1.4	-1.1	2.6	0.3	2.6	0.8	2.1	1.0	1.8
(5)	1.3	-0.7	6.2	-1.1	5.2	0.4	3.5	0.6	1.7
Free Energy (Quasi-RRHO Approximation)[52]									
(1)	9.5	9.1	9.8	9.2	9.6	9.5	9.5	9.5	9.5
(2)	0.9	-0.1	2.4	0.4	2.0	0.7	1.4	0.6	1.2
(3)	2.4	1.5	2.7	1.5	2.8	2.2	2.6	2.3	2.5
(4)	1.0	-0.5	2.0	0.3	1.7	0.7	1.3	0.8	1.2
(5)	1.3	-0.5	5.3	-0.3	4.3	0.8	2.7	0.8	1.5
Free Energy (Quasi-harmonic Approximation)[51]									
(1)	9.7	9.6	9.8	9.7	9.7	9.7	9.7	9.7	9.7
(2)	1.0	0.1	2.3	0.7	1.8	0.9	1.5	0.8	1.3
(3)	2.4	1.6	2.8	2.3	2.6	2.4	2.5	2.4	2.5
(4)	0.8	-0.3	1.8	0.3	1.3	0.6	0.9	0.6	0.9
(5)	1.2	-0.6	4.7	-0.1	3.9	0.6	2.3	0.8	1.4

[a] Rotationally averaged energy differences using a (175,974) grid.

Table 1 contains grid-converged energies, enthalpies, and free energies (using the RRHO, quasi-RRHO, and quasi-harmonic approximations)[51-52] for reactions 1-5 as well as the minimum and maximum values that can be obtained by varying one or both molecular orientations using four popular integration grids. For several of these reactions there are large variations in the relative electronic energies, particularly using the SG-1 grid. While these variations are due to previously documented grid errors, their implications for predictions of reaction outcomes should not be overlooked. For instance, using the SG-1 grid, the overall sign of the electronic energy difference between the two stereocontrolling TS structures for reaction 4 can vary. In other words, using this grid one cannot confidently predict which of the stereoisomeric products will be preferentially formed. As reported by Head-Gordon and co-workers[26] for atomization

energies, these errors in E are essentially converged by the (99,590) grid. Variations in relative enthalpies are slightly larger, and there are troublingly large swings in computed values using both the SG-1 and (75,302) grids. For instance, the relative enthalpy of the regiocontrolling TS structures for reaction 5 can fall anywhere between 0.8 and 2.1 kcal mol^{-1}, preventing any quantitative prediction of regioselectivity.

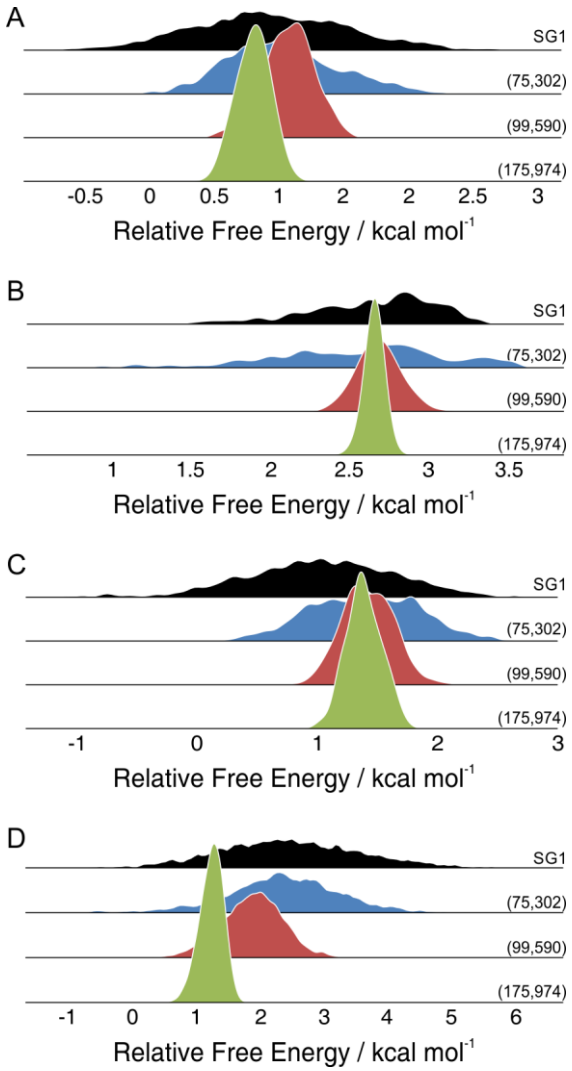

Figure 2. Distribution of RRHO free energy differences across all combinations of sampled orientations for the two structures for reactions (A) 2, (B) 3, (C) 4, and (D) 5.

Variations in free energies are even larger and more slowly convergent with respect to grid size. Moreover, while the quasi-RRHO and quasi-harmonic approximations reduce the ranges of free energy differences, they remain significant (see Table 1). To provide a better feel for the spread of possible computed free energy differences using different popular grids, the

distributions of free energy values across different orientations for reactions 2-5 are shown in Figure 2. In all cases, the spread of free energy differences computed using the SG-1 and (75,302) grids are substantial. Moreover, for some of these reactions one can obtain *qualitatively* different results using a given level of theory by considering different molecular orientations. For example, using a (75,302) grid the computed torsional free energy barrier for reaction 3 can be anywhere from 0.8 kcal mol^{-1} to 3.5 kcal mol^{-1}, corresponding to two orders of magnitude in terms of reaction rate. Even worse, the relative free energies of the HIV integrase inhibitor **1**, relative its diastereomer (reaction 2), can vary from –1.1 kcal mol^{-1} to +2.6 kcal mol^{-1} using the SG-1 grid. This is particularly important, because it was found experimentally that the biologically active form of this potential drug (**1**) was the less stable diastereomer, necessitating the development of a complex stereoselective synthesis of the desired molecule.[60]

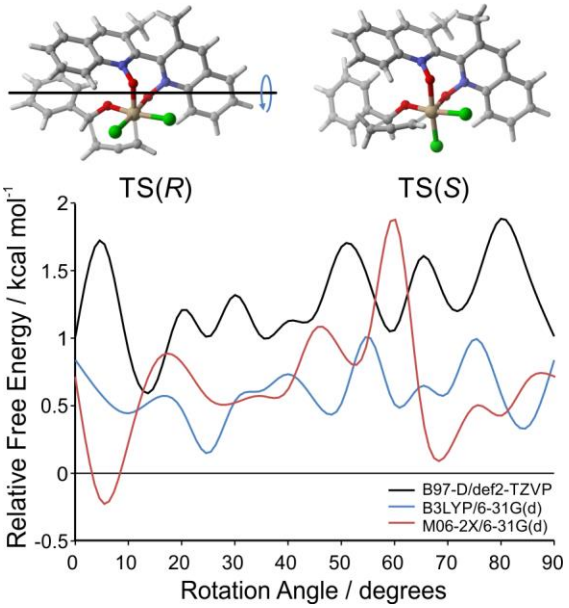

Figure 3. RRHO free energy difference between the stereocontrolling TS structures for reaction 4 for three levels of theory using a pruned (75,302) grid for different orientations of TS(R) and TS(S) in its standard orientation.

The variations in $\Delta\Delta G^{\ddagger}$ for reactions 4 and 5 are particularly large, which does not bode well for predictions of selectivity. For example, for reaction 4, RRHO $\Delta\Delta G^{\ddagger}$ values at the B97-D/def2-TZVP level of theory using a pruned (75,302) grid range from 0.3 kcal mol^{-1} to 2.6 kcal mol^{-1} depending on the TS orientations. In other words, one can predict selectivities for this reaction that range anywhere from 62:38 to 99:1 by choosing different molecular orientations. Using the SG-1 grid, predicted selectivities can range from 14:86 to 99:1. Even with the (99,590) and (175,974) grids, $\Delta\Delta G^{\ddagger}$ still varies by 1.2 and 0.8 kcal mol^{-1}, respectively, leading to

unacceptably large uncertainties in predicted enantioselectivities for this simple organocatalytic reaction. Similar variations in $\Delta\Delta G^{\ddagger}$ for this reaction arise using other popular functionals paired with a pruned (75,302) grid (See Figure 3). In the standard orientation (rotation angle of 0°) these three DFT methods provide consistent $\Delta\Delta G^{\ddagger}$ values of 0.85 ± 0.15 kcal mol^{-1}. However, rotating TS(R) by only 5° results in divergent stereoselectivity predictions. The result is that the molecular orientation has a far greater impact on the predicted selectivity of this reaction than the choice of exchange-correlation functional.

Variations in the free energy difference between the regiocontrolling TS structures for reaction 5 span more than 6 kcal mol^{-1} for the SG-1 and (75,302) grids. For instance, using the (75,302) grid, this free energy difference can fall anywhere from –1.1 to +5.2 kcal mol^{-1}. Figure 4 shows the energy, enthalpy, and RRHO free energy of TS(C_7) in a fixed orientation relative to different orientations of TS(C_2) using a pruned (75,302) grid. By varying just one TS structure, $\Delta\Delta G^{\ddagger}$ values fluctuate between ±1 kcal mol^{-1}, again highlighting the sensitivity of DFT free energies to even small changes in orientation. Even with the very large (174,975) grid the $\Delta\Delta G^{\ddagger}$ values for reaction 5 can vary by more than 1 kcal mol^{-1}.

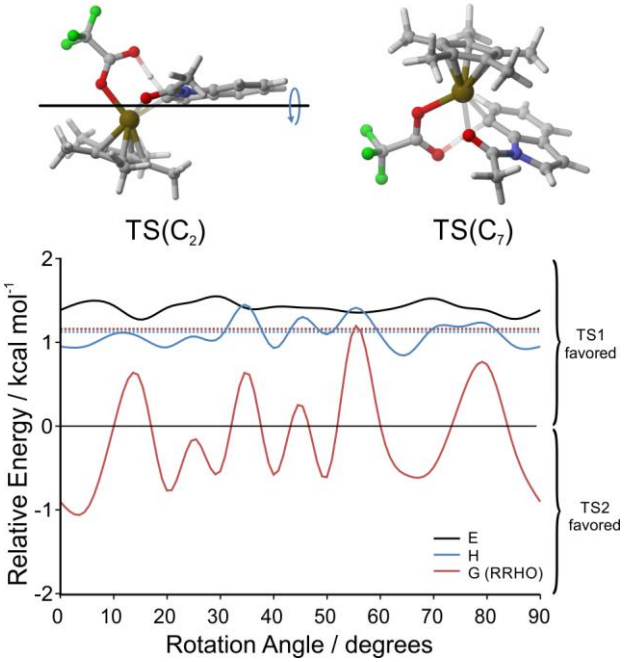

Figure 4. M06/6-31G(d,p)/LANL2DZ energy (E), enthalpy (H), and RRHO free energy (G) of TS(C_7) relative to TS(C_2) using a pruned (75,302) grid for different orientations of TS(C_2) and the pictured orientation of TS(C_7), which is rotated 15° from the standard orientation (grid-converged values indicated with dotted lines).

The lack of rotational invariance of DFT energies, gradients, and vibrational frequencies is widely acknowledged,[33-35] and documentation for many quantum chemistry packages include caveats regarding the sensitivity of vibrational frequencies to integration grids. For instance, starting with Gaussian98, a (99,590) grid has been recommended for computing 'very low frequency modes.' Similarly, the Orca manual advises users to assess the convergence of vibrational frequencies with respect to integration grid. Unfortunately, these sage pieces of advice seem to have gone largely unheeded among users, as evidenced by a lack of discussion of grids in otherwise comprehensive recent reviews covering the challenges of accurately modeling complex organic and organometallic systems.[2,10-12]

One means of dealing with the lack of rotational invariance is to use the 'standard orientation' in all computations. Equivalently, the atom-centered integration grids can be rotated with the molecule.[34] Along the same lines, the Orca manual warns against the use of 'grossly different orientations' when computing relative energies of similar molecules. These approaches all rest on the assumption that similar orientations will minimize grid errors in computed free energies. Table 2 lists errors in RRHO free energies for reactions 1-5 using the standard orientation, relative to grid-converged values. In most cases, the errors in the standard orientation are large, particularly for the smaller grids. For example, using the SG-1 grid, $\Delta\Delta G^{\ddagger}$ for reaction 5 is 1.5 kcal mol^{-1} from the grid-converged value of 1.3 kcal mol^{-1}. While the errors are smaller for the other reactions and grids, they are not negligible until reaching the (175,974) grid. In other words, the use of a standard orientation (or equivalently, rotating the atom-centered grids with the molecule) does not minimize these grid errors. Similarly, the use of 'similar orientations' does not necessarily lead to error cancelation. This can be seen explicitly in Figure 5, which shows the relative free energies of the two regiocontrolling TS structures for reaction 5 as they are rotated simultaneously around the indicated axes starting from their respective standard orientations. Even using a (99,590) grid, there is more than 2 kcal mol^{-1} variation in the free energy difference between these regiocontrolling TS structures.

Table 2. Errors in RRHO free energy differences for reactions 1-5 using the standard orientation, relative to grid-converged values, in kcal mol^{-1}.

Reaction	SG-1	(75,302)	(99,590)	(175,974)
(1)	0.5	-0.1	0.0	0.0
(2)	0.8	-0.1	0.2	-0.1
(3)	0.0	-0.8	-0.1	0.0
(4)	-0.9	-0.4	0.3	0.0
(5)	1.5	0.6	0.6	-0.2

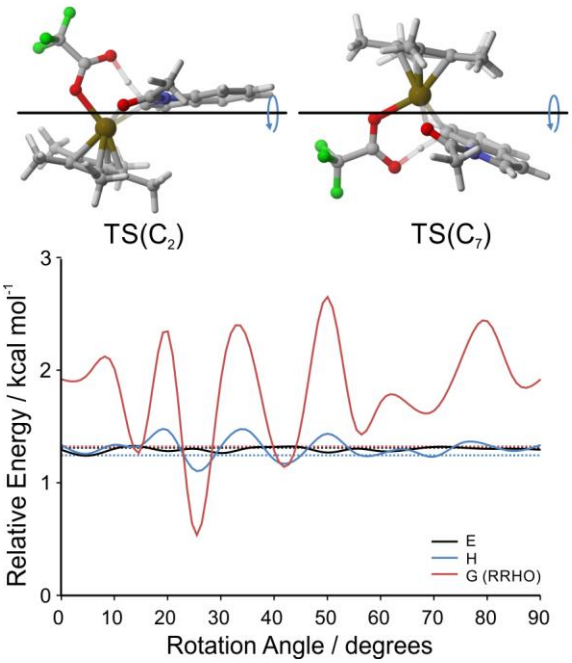

Figure 5. M06/6-31G(d,p)/LANL2DZ energy (E), enthalpy (H), and RRHO free energy (G) of $TS(C_7)$ relative to $TS(C_2)$ for simultaneous rotation of $TS(C_2)$ and $TS(C_7)$ around the indicated axis starting from the standard orientation (pictured) using a pruned (99,590) grid. Grid-converged values indicated with dotted lines.

Conclusions

The evaluation of accurate relative free energies is vital for many applications of quantum chemistry to (bio-)organic and organometallic systems.[1-9] We showed that the lack of rotational invariance of popular integration grids can result in large uncertainties in DFT-computed free energy differences, with SG-1 and pruned (75,302) grids leading to errors exceeding 5 kcal mol^{-1} in relative free energies for some systems. As the default in Gaussian09 and many other codes, the latter grid is particularly widely used. While the reactions in Scheme 1 were chosen to highlight these errors, they are not atypical. Consequently, errors of this magnitude are potentially widespread among modern DFT applications and can easily overshadow chemically

meaningful free energy differences. In some cases, the outcomes of reactions predicted based on free energies using a given level of DFT theory can vary *qualitatively* depending on molecular orientation. Relative enthalpies, on the other hand, are far less sensitive to grids, and often provide closer agreement with experiment than ostensibly more physically meaningful free energies. In fact, one hallmark of the grid errors detailed above is a qualitative difference between relative enthalpies and free energies.

The underlying source of these errors is the unphysically large contribution of low-frequency vibrational modes to the entropic component of the free energy in the standard RRHO treatment. To this end, the quasi-harmonic and quasi-RRHO approximations[51-52] reduce, but do not eliminate, these grid errors. At the same time, despite continued advances in more rigorous treatments of the entropic contributions of low-frequency vibrational modes,[61-62] such approaches are still impractical for the organic and organometallic systems most often subject to DFT computations. Baik *et al.*[11] recently warned of the unphysical contributions of low frequency vibrational modes to the free energies in organometallic systems, showing that rotations of a Cp ring in a Rh-complex can lead to variations of nearly 2 kcal mol^{-1} in the free energy. The grid errors discussed above are arguably more alarming, because they concern larger variations in free energies for rotations of the entire molecule.

The good news is that these errors are reduced substantially using a (99,590) grid in many cases. Consequently, this grid (which is the default in Gaussian16)[63] should be considered a minimal grid when using DFT to compute free energies of any system with low-frequency vibrational modes (< 100 cm^{-1}). However, given that errors of ~1 kcal mol^{-1} remain for some systems even with larger grids, we implore users to compute free energies for several molecular orientations[64] using multiple integration grids in order to gauge the magnitude of grid errors and to guide the choice of the most appropriate integration grid for a given problem. Quantum chemistry applications always require choices between accuracy and computational expediency, and users must strive to identify and minimize major sources of errors. Herein, we highlighted the choice of integration grid as an often-overlooked source of error in DFT free energy computations. As long as predictions and interpretations based on DFT computed free energies are made with these potential errors in mind, DFT remains a powerful and indispensable tool for analyzing and even predicting the outcome of organic and organometallic reactions.

Theoretical Methods

Gas-phase energies, enthalpies (298K), and free energies (298K) for each energy minimum or TS structure for reactions 1-5 were computed for 25 (for reactions 2-4) or 50 (for reactions 1 and 5) representative orientations using four pruned[65] integration grids: (50,194), (75,302), (99,590), and (175,974) [the latter uses a (250,974) grid for Ir], accessible in Gaussian via the grid keywords 'SG1grid,' 'Fine,' 'Ultrafine,' and 'Superfine.' These orientations were generated by performing independent rigid body rotations around the three principle axes in 10° (or 5°) increments up to 80° (or 85°) starting from the respective standard orientations using AaronTools.[66] For reaction 1, only the orientation of 2-butyne was varied, because the free energy of 1,3-butadiene is essentially constant across different orientations. For each orientation, the geometry was fully optimized using the corresponding integration grid such that the maximum and RMS gradients were below 1.5 x 10^{-5} and 1.0 x 10^{-5} hartree/bohr, respectively. Harmonic vibrational frequencies were then computed via analytic second derivatives. By default, Gaussian uses smaller grids in the solution of the CPHF equations than requested for the SCF equations (the 'Fine' grid for a 'superfine' SCF grid, 'SG-1' for the 'ultrafine' SCF grid, and 'coarse' for the others); however, the use of larger grids for the CPHF equations does not appear to eliminate these errors (see SI Figure S3). It should also be noted that if geometries were not re-optimized at each orientation, the observed variations in enthalpies and free energies were even larger and there were often many superfluous imaginary vibrational modes. Grid-converged values of energies, enthalpies, and free energies were obtained by averaging the corresponding quantity using a (175,974) grid across all combinations of sampled orientations. In Table 1, the minimum and maximum energy differences correspond to the extreme energy differences across all sampled orientations. For orientations for which the correct rotational symmetry number was not automatically recognized, we manually appended the corresponding correction to the entropy. Quasi-RRHO and quasi-harmonic free energies were computed using AaronTools.[66]

The data in Table 1 for reactions 1-4 were computed at the B97-D/def2-TZVP level of theory using density fitting. It should be noted that the documented grid errors are independent of whether density fitting is used (see SI Figure S4). Additional data for reaction 4 were also computed using B3LYP/6-31G(d) and M06-2X/6-31G(d) for Figure 3. Data for reaction 5 were computed using M06 paired with the LANL2DZ/HayWadt basis set/ECP on Ir and the 6-31G(*d,p*) basis set on all other atoms,[43,67] following Ref 59. For reaction 4, initial TS structures

were taken from Ref 56; initial TS structures for reaction 5 were taken from Ref 59. Predicted selectivities for reactions 4 and 5 assume Curtin-Hammett conditions. The computations presented above were performed using Gaussian09;[36] selected data were also computed using Orca[68] (see SI). Molecular structure figures were generated using CYLView.[69]

Acknowledgments

This work was supported by the National Science Foundation (Grant CHE-1665407) and conducted with high performance computing resources provided by the Georgia Advanced Computing Resource Center (http://gacrc.uga.edu). We thank D. Maziotti, R. S. Paton, P.-O. Norrby, C. E. Webster, M. L. Coote, K. Jorner, and F. Schoenebeck as well as E. N. Brothers and participants in the conference Emerging Tools for Designing Practical Next Generation Catalysts at TAMUQ for fruitful discussions. A. J. Schaefer is thanked for assistance regarding reaction 5.

Supporting Information Available: Additional computational data and figures, absolute energies, Cartesian coordinates.

References

1. Houk, K. N.; Cheong, P. H., Computational prediction of small-molecule catalysts. *Nature* **2008,** *455*, 309-313.
2. Sperger, T.; Sanhueza, I. A.; Kalvet, I.; Schoenebeck, F., Computational Studies of Synthetically Relevant Homogeneous Organometallic Catalysis Involving Ni, Pd, Ir, and Rh: An Overview of Commonly Employed DFT Methods and Mechanistic Insights. *Chem. Rev.* **2015,** *115*, 9532-9586.
3. Peng, Q.; Duarte, F.; Paton, R. S., Computing organic stereoselectivity - from concepts to quantitative calculations and predictions. *Chem. Soc. Rev.* **2016,** *45*, 6093-6107.
4. Lam, Y. H.; Grayson, M. N.; Holland, M. C.; Simon, A.; Houk, K. N., Theory and Modeling of Asymmetric Catalytic Reactions. *Acc. Chem. Res.* **2016,** *49*, 750-762.
5. Sperger, T.; Sanhueza, I. A.; Schoenebeck, F., Computation and Experiment: A Powerful Combination to Understand and Predict Reactivities. *Acc. Chem. Res.* **2016,** *49*, 1311-1319.
6. Houk, K. N.; Liu, F., Holy Grails for Computational Organic Chemistry and Biochemistry. *Acc. Chem. Res.* **2017,** *50*, 539-543.
7. Poree, C.; Schoenebeck, F., A Holy Grail in Chemistry: Computational Catalyst Design: Feasible or Fiction? *Acc. Chem. Res.* **2017,** *50*, 605-608.
8. Maji, R.; Mallojjala, S. C.; Wheeler, S. E., Chiral phosphoric acid catalysis: from numbers to insights. *Chem. Soc. Rev.* **2018,** *47*, 1142-1158.
9. Ahn, S.; Hong, M.; Sundararajan, M.; Ess, D. H.; Baik, M. H., Design and Optimization of Catalysts Based on Mechanistic Insights Derived from Quantum Chemical Reaction Modeling. *Chem. Rev.* **2019,** *119*, 6509-6560.

10. Tsang, A. S.; Sanhueza, I. A.; Schoenebeck, F., Combining experimental and computational studies to understand and predict reactivities of relevance to homogeneous catalysis. *Chem. Eur. J.* **2014,** *20*, 16432-16441.
11. Ryu, H.; Park, J.; Kim, H. K.; Park, J. Y.; Kim, S. T.; Baik, M. H., Pitfalls in Computational Modeling of Chemical Reactions and How To Avoid Them. *Organometallics* **2018,** *37*, 3228-3239.
12. Harvey, J. N.; Himo, F.; Maseras, F.; Perrin, L., Scope and Challenge of Computational Methods for Studying Mechanism and Reactivity in Homogeneous Catalysis. *ACS Catal.* **2019**, 6803-6813.
13. Termath, V.; Sauer, J., Optimized molecular integration schemes for density functional theory ab initio molecular dynamics simulations. *Chem. Phys. Lett.* **1996,** *255*, 187-194.
14. Dressler, S.; Thiel, W., Anharmonic force fields from density functional theory. *Chem. Phys. Lett.* **1997,** *273*, 71-78.
15. Martin, J. M. L.; Bauschlicher, C. W.; Ricca, A., On the integration accuracy in molecular density functional theory calculations using Gaussian basis sets. *Comput. Phys. Commun.* **2001,** *133*, 189-201.
16. Johnson, E. R.; Wolkow, R. A.; DiLabio, G. A., *Chem. Phys. Lett.* **2004,** *394*, 334-338.
17. Papas, B. N.; Schaefer, H. F., Concerning the precision of standard density functional programs: GAUSSIAN, MOLPRO, NWCHEM, Q-CHEM, and GAMESS. *Journal of Molecular Structure-Theochem* **2006,** *768*, 175-181.
18. Grafenstein, J.; Izotov, D.; Cremer, D., Avoiding singularity problems associated with meta-GGA (generalized gradient approximation) exchange and correlation functionals containing the kinetic energy density. *J. Chem. Phys.* **2007,** *127*, 214103.
19. Grafenstein, J.; Cremer, D., Efficient density-functional theory integrations by locally augmented radial grids. *J. Chem. Phys.* **2007,** *127*, 164113.
20. Jiménez-Hoyos, C. A.; Janesko, B. G.; Scuseria, G. E., Evaluation of range-separated hybrid density functionals for the prediction of vibrational frequencies, infrared intensities, and Raman activitiesw. *Phys. Chem. Chem. Phys.* **2008,** *10*, 6621-6629.
21. Johnson, E. R.; Becke, A. D.; Sherrill, C. D.; DiLabio, G. A., Oscillations in meta-generalized-gradient approximation potential energy surfaces for dispersion-bound complexes. *J. Chem. Phys.* **2009,** *131*, 034111.
22. Fusti-Molnar, L.; He, X.; Wang, B.; Merz, K. M., Jr., Further analysis and comparative study of intermolecular interactions using dimers from the S22 database. *J. Chem. Phys.* **2009,** *131*, 065102.
23. Csonka, G. I.; French, A. D.; Johnson, G. P.; Stortz, C. A., Evaluation of Density Functionals and Basis Sets for Carbohydrates. *J. Chem. Theory Comput.* **2009,** *5*, 679-692.
24. Wheeler, S. E.; Houk, K. N., Integration Grid Errors for Meta-GGA-Predicted Reaction Energies: Origin of Grid Errors for the M06 Suite of Functionals. *J. Chem. Theory Comput.* **2010,** *6*, 395-404.
25. Mardirossian, N.; Head-Gordon, M., ωB97X-V: a 10-parameter, range-separated hybrid, generalized gradient approximation density functional with nonlocal correlation, designed by a survival-of-the-fittest strategy. *Phys. Chem. Chem. Phys.* **2014,** *16*, 9904-9924.
26. Mardirossian, N.; Head-Gordon, M., How Accurate Are the Minnesota Density Functionals for Noncovalent Interactions, Isomerization Energies, Thermochemistry, and Barrier Heights Involving Molecules Composed of Main-Group Elements? *J. Chem. Theory Comput.* **2016,** *12*, 4303-4325.

27. Mardirossian, N.; Head-Gordon, M., ωB97M-V: A combinatorially optimized, range-separated hybrid, meta-GGA density functional with VV10 nonlocal correlation. *J. Chem. Phys.* **2016,** *144*, 214110.
28. Wang, Y.; Jin, X.; Yu, H. S.; Truhlar, D. G.; He, X., Revised M06-L functional for improved accuracy on chemical reaction barrier heights, noncovalent interactions, and solid-state physics. *Proc. Natl. Acad. Sci. U. S. A.* **2017,** *114*, 8487-8492.
29. Zhao, Y.; Truhlar, D. G., The M06 Suite of Density Functionals for Main Group Thermochemistry, Thermochemical Kinetics, Noncovalent interactions, Excited States, and Transition Elements: Two New Functionals and Systematic Testing of Four M06 Functionals and Twelve Other Functionals. *Theo. Chem. Acc.* **2008,** *120*, 215-241.
30. Gill, P. M. W.; Johnson, B. G.; Pople, J. A., A Standard Grid for Density-Functional Calculations. *Chem. Phys. Lett.* **1993,** *209*, 506-512.
31. Wang, Y.; Verma, P.; Jin, X.; Truhlar, D. G.; He, X., Revised M06 density functional for main-group and transition-metal chemistry. *Proc. Natl. Acad. Sci. U. S. A.* **2018,** *115*, 10257-10262.
32. Dasgupta, S.; Herbert, J. M., Standard grids for high-precision integration of modern density functionals: SG-2 and SG-3. *J. Comput. Chem.* **2017,** *38*, 869-882.
33. Jones, R. S.; Mintmire, J. W.; Dunlap, B. I., Geometry Optimization Using Local-Density Functional Methods - Numerical Aspects. *Int. J. Quantum Chem.* **1988,** *34*, 77-84.
34. Johnson, B. G.; Gill, P. M. W.; Pople, J. A., A Rotationally Invariant Procedure for Density-Functional Calculations. *Chem. Phys. Lett.* **1994,** *220*, 377-384.
35. Johnson, B. G., Analytic second derivatives of the gradient-corrected density functional energy. Effect of quadrature weight derivatives. *Chem. Phys. Lett.* **1993,** *216*, 133-140.
36. Frisch, M.; Trucks, G.; Schlegel, H.; Scuseria, G.; Robb, M.; Cheeseman, J.; Scalmani, G.; Barone, V.; Mennucci, B.; Petersson, G.; Nakatsuji, H.; Caricato, M.; Li, X.; Hratchian, H.; Izmaylov, A.; Bloino, J.; Zheng, G.; Sonnenberg, J.; Hada, M.; Ehara, M.; Toyota, K.; Fukuda, R.; Hasegawa, J.; Ishida, M.; Nakajima, T.; Honda, Y.; Kitao, O.; Nakai, H.; Vreven, T.; Montgomery, J., JA; Peralta, J.; Ogliaro, F.; Bearpark, M.; Heyd, J.; Brothers, E.; Kudin, K.; Staroverov, V.; Keith, T.; Kobayashi, R.; Normand, J.; Raghavachari, K.; Rendell, A.; Burant, J.; Iyengar, S.; Tomasi, J.; Cossi, M.; Rega, N.; Millam, J.; Klene, M.; Knox, J.; Cross, J.; Bakken, V.; Adamo, C.; ramillo, J.; Gomperts, R.; Stratmann, R.; Yazyev, O.; Austin, A.; Cammi, R.; Pomelli, C.; Ochterski, J.; Martin, R.; Morokuma, K.; Zakrzewski, V.; Voth, G.; Salvador, P.; Dannenberg, J.; Dapprich, S.; Daniels, A.; Farkas, O.; Foresman, J.; Ortiz, J.; Cioslowski, J.; Fox, D. *Gaussian 09, Revision D.01*, Gaussian, Inc.: 2009.
37. Lebedev, V. I.; Laikov, D. N., *Dokl. Math.* **1999,** *59*, 477.
38. Grimme, S., Semiempirical GGA-type density functional constructed with a long-range dispersion correction. *J. Comput. Chem.* **2006,** *27*, 1787-1799.
39. Becke, A., Density-Functional Thermochemistry. V. Systematic Optimization of Exchange-Correlation Functionals. *J. Chem. Phys.* **1997,** *107*, 8554-8560.
40. Becke, A. D., Density-functional thermochemistry. III. The role of exact exchange. *J. Chem. Phys.* **1993,** *98*, 5648-5652.
41. Perdew, J. P.; Burke, K.; Ernzerhof, M., Generalized Gradient Approximation Made Simple. *Phys. Rev. Lett.* **1996,** *77*, 3865-3868.
42. Chai, J. D.; Head-Gordon, M., Long-range corrected hybrid density functionals with damped atom-atom dispersion corrections. *Phys. Chem. Chem. Phys.* **2008,** *10*, 6615-6620.

43. Zhao, Y.; Truhlar, D. G., The M06 suite of density functionals for main group thermochemistry, thermochemical kinetics, noncovalent interactions, excited states, and transition elements: two new functionals and systematic testing of four M06-class functionals and 12 other functionals. *Theor. Chem. Acc.* **2008,** *120*, 215-241.
44. Dunning, T. H., Gaussian basis sets for use in correlated molecular calculations. I. The atoms boron through neon and hydrogen. *J. Chem. Phys.* **1989,** *90*, 1007-1023.
45. Weigend, F.; Ahlrichs, R., Balanced basis sets of split valence, triple zeta valence and quadruple zeta valence quality for H to Rn: Design and assessment of accuracy. *Phys. Chem. Chem. Phys.* **2005,** *7*, 3297-3305.
46. It should be noted that variations in low frequency modes appear to be converge more rapidly with grid size using Orca (see SI Figure S2).
47. McClurg, R. B., Comment on "The hindered rotor density-of-states interpolation function" [J. Chem. Phys. 106, 6675 (1997)] and "The hindered rotor density-of-states" [J. Chem. Phys. 108, 2314 (1998)]. *J. Chem. Phys.* **1999,** *111*, 7163-7164.
48. McClurg, R. B.; Flagan, R. C.; Goddard, W. A., The hindered rotor density-of-states interpolation function. *J. Chem. Phys.* **1997,** *106*, 6675-6680.
49. Ayala, P. Y.; Schlegel, H. B., Identification and treatment of internal rotation in normal mode vibrational analysis. *J. Chem. Phys.* **1998,** *108*, 2314-2325.
50. Chuang, Y. Y.; Truhlar, D. G., Statistical thermodynamics of bond torsional modes. *J. Chem. Phys.* **2000,** *112*, 1221-1228.
51. Ribeiro, R. F.; Marenich, A. V.; Cramer, C. J.; Truhlar, D. G., Use of solution-phase vibrational frequencies in continuum models for the free energy of solvation. *J. Phys. Chem. B* **2011,** *115*, 14556-14562.
52. Grimme, S., Supramolecular binding thermodynamics by dispersion-corrected density functional theory. *Chem. Eur. J.* **2012,** *18*, 9955-9964.
53. Throughout, we consider any vibrational frequency below 100 cm-1 to be a 'low frequency vibrational mode.'
54. Haddad, N.; Mangunuru, H. P. R.; Fandrick, K. R.; Qu, B.; Sieber, J. D.; Rodriguez, S.; Desrosiers, J. N.; Patel, N. D.; Lee, H.; Kurouski, D.; Grinberg, N.; Yee, N. K.; Song, J. H. J.; Senanayake, C. H., Reengineered BI-DIME Ligand Core Based on Computer Modeling to Increase Selectivity in Asymmetric Suzuki-Miyaura Coupling for the Challenging Axially Chiral HIV Integrase Inhibitor. *Adv. Synth. Catal.* **2016,** *358*, 3522-3527.
55. Lu, T.; Zhu, R.; An, Y.; Wheeler, S. E., Origin of enantioselectivity in the propargylation of aromatic aldehydes catalyzed by helical N-oxides. *J. Am. Chem. Soc.* **2012,** *134*, 3095-3102.
56. Doney, A. C.; Rooks, B. J.; Lu, T. X.; Wheeler, S. E., Design of Organocatalysts for Asymmetric Propargylations through Computational Screening. *ACS Catal.* **2016,** *6*, 7948-7955.
57. Wheeler, S. E.; Seguin, T. J.; Guan, Y.; Doney, A. C., Noncovalent Interactions in Organocatalysis and the Prospect of Computational Catalyst Design. *Acc. Chem. Res.* **2016,** *49*, 1061-1069.
58. Nakajima, M.; Saito, M.; Hashimoto, S., Selective synthesis of optically active allenic and homopropargylic alcohols from propargyl chloride. *Tetrahedron-Asymmetry* **2002,** *13*, 2449-2452.
59. Kim, Y.; Park, Y.; Chang, S., Delineating Physical Organic Parameters in Site-Selective C-H Functionalization of Indoles. *ACS Cent Sci* **2018,** *4*, 768-775.

60. Fandrick, K. R.; Li, W.; Zhang, Y.; Tang, W.; Gao, J.; Rodriguez, S.; Patel, N. D.; Reeves, D. C.; Wu, J. P.; Sanyal, S.; Gonnella, N.; Qu, B.; Haddad, N.; Lorenz, J. C.; Sidhu, K.; Wang, J.; Ma, S.; Grinberg, N.; Lee, H.; Tsantrizos, Y.; Poupart, M. A.; Busacca, C. A.; Yee, N. K.; Lu, B. Z.; Senanayake, C. H., Concise and Practical Asymmetric Synthesis of a Challenging Atropisomeric HIV Integrase Inhibitor. *Angew Chem Int Ed Engl* **2015,** *54*, 7144-7148.
61. Jasper, A. W.; Gruey, Z. B.; Harding, L. B.; Georgievskii, Y.; Klippenstein, S. J.; Wagner, A. F., Anharmonic Rovibrational Partition Functions for Fluxional Species at High Temperatures via Monte Carlo Phase Space Integrals. *J. Phys. Chem. A* **2018,** *122*, 1727-1740.
62. Wu, J.; Ning, H.; Xu, X.; Ren, W., Accurate entropy calculation for large flexible hydrocarbons using a multi-structural 2-dimensional torsion method. *Phys. Chem. Chem. Phys.* **2019,** *21*, 10003-10010.
63. Frisch, M. J.; Trucks, G. W.; Schlegel, H. B.; Scuseria, G. E.; Robb, M. A.; Cheeseman, J. R.; Scalmani, G.; Barone, V.; Petersson, G. A.; Nakatsuji, H.; Li, X.; Caricato, M.; Marenich, A. V.; Bloino, J.; Janesko, B. G.; Gomperts, R.; Mennucci, B.; Hratchian, H. P.; Ortiz, J. V.; Izmaylov, A. F.; Sonnenberg, J. L.; Williams; Ding, F.; Lipparini, F.; Egidi, F.; Goings, J.; Peng, B.; Petrone, A.; Henderson, T.; Ranasinghe, D.; Zakrzewski, V. G.; Gao, J.; Rega, N.; Zheng, G.; Liang, W.; Hada, M.; Ehara, M.; Toyota, K.; Fukuda, R.; Hasegawa, J.; Ishida, M.; Nakajima, T.; Honda, Y.; Kitao, O.; Nakai, H.; Vreven, T.; Throssell, K.; Montgomery Jr., J. A.; Peralta, J. E.; Ogliaro, F.; Bearpark, M. J.; Heyd, J. J.; Brothers, E. N.; Kudin, K. N.; Staroverov, V. N.; Keith, T. A.; Kobayashi, R.; Normand, J.; Raghavachari, K.; Rendell, A. P.; Burant, J. C.; Iyengar, S. S.; Tomasi, J.; Cossi, M.; Millam, J. M.; Klene, M.; Adamo, C.; Cammi, R.; Ochterski, J. W.; Martin, R. L.; Morokuma, K.; Farkas, O.; Foresman, J. B.; Fox, D. J. *Gaussian 16 Rev. B.01*, Wallingford, CT, 2016.
64. In Gaussian, the keyword 'nosymm' prevents the system from being automatically rotated to the 'standard orientation.'
65. The use of an unpruned (75,302) grid results in no noticeable reduction in errors compared to the pruned version; see SI Figure S3.
66. Guan, Y.; Ingman, V. M.; Rooks, B. J.; Wheeler, S. E., AARON: An Automated Reaction Optimizer for New Catalysts. *J. Chem. Theory Comput.* **2018,** *14*, 5249-5261.
67. Hay, P. J.; Wadt, W. R., Ab initio effective core potentials for molecular calculations. Potentials for the transition metal atoms Sc to Hg. *J. Chem. Phys.* **1985,** *82*, 270-283.
68. Neese, F., Software update: the ORCA program system, version 4.0. *Wiley Interdisciplinary Reviews-Computational Molecular Science* **2018,** *8*.
69. Legault, C. Y. *CYLview, 1.0b*, Université de Sherbrooke: 2009.

TOC Figure

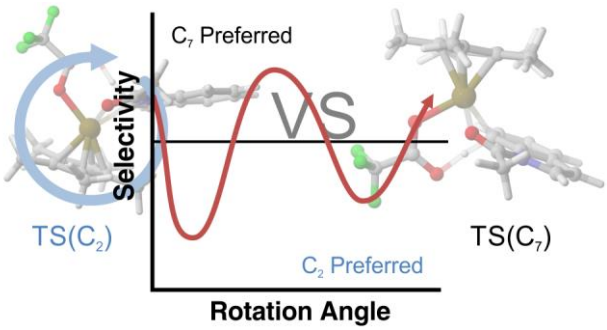
C7 Preferred
VS
Selectivity
TS(C2)
TS(C7)
C2 Preferred
Rotation Angle